International Journal of Remote Sensing & Geoscience (IJRSG)
www.ijrsg.com

2D AND 3D IMAGE FOR SYNTHETIC APERTURE RADAR

Dr. Ali Nassib
Department of Electrical Engineering
University of Dayton
Email: nassiba1@udayton.edu

Abstract

This paper presents a unique way of reconstructing 2D and 3D SAR image. The current SAR imaging algorithms is modeled as if the target of interest consists of collection of radiating discrete set of points known as point source model. This model is good enough as long the orientation of the target is not that important. But in this paper we employed a special technique known as dipole model which captures the orientation of the target by assuming the target consists of a collection of infinitesimally small dipoles. The orientation of each dipole is accounted in a dyadic contrast function. The image of the target is reconstructed by acquiring the reflectivity function from the 2D and the 3D simulated data.

I. Introduction

Synthetic Aperture Radar known as SAR is a high resolution airborne and spaceborne imaging system which generates its own source to illuminate the target of interest and then collects the backscattered signals coherently by using the range Doppler algorithm (RDA). When these backscattered signals are analyzed together by coherent combination they generate high resolution image. SAR utilizes the movement of the antenna platform by artificially creating very long linear array with respect to the target. The reason for creating long linear array is to be able to separate targets that are closely spaced in cross rang as shown in equation (1) below.

SAR generates two dimensional high resolution image of a target by using the information of both down range direction and cross range direction. Range resolution is acquired either using short pulse or pulse compression where the cross-range resolution is acquired Doppler history of different parts of the target as shown equation 1&2.

$$\overbrace{r = \frac{c_0}{2B}}^{\text{Range resolution}} \qquad (1)$$

$$\overbrace{\Delta r = \frac{\lambda_0}{2 * \Delta\theta}}^{\text{Cross range resolution}} \qquad (2)$$

SAR is coherent radar which sends out a set of pulses that are digitally sampled and coherently integrated to increase the signal to noise ratioas can be seen in equation (3)because the signal returns are almost the same from pulse to pulse where the noise is different, in other wards independent from pulse to pulse.

$$\overbrace{\frac{S}{N} = \frac{P_t G_t^{\,2} \lambda^2 \sigma}{(4\pi)^3 R^4 k T_0 B F_n L}}^{\text{Signal to noise ratio}} \qquad (3)$$

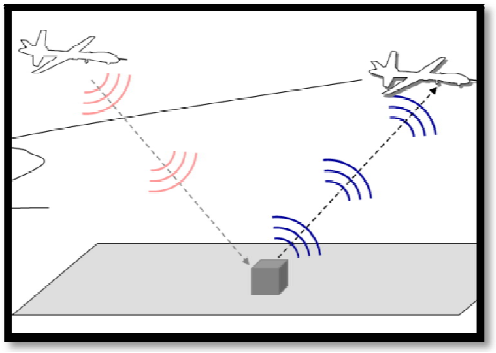

Figure 1: SAR imaging attempts to reconstruct an image of stationary target.

SAR has broad range Applications of SAR such as intelligence, and reconnaissance, interferometry, foliage penetration, moving target indication, and environmental monitoring and so on. SAR consist of three types modes of operation strip-map, spotlight, and scan-SAR. In strip-map mode, the antenna boresight is in a fixed position and the backscattered signal is collected along the flight path. Spotlight mode, the radar tracks and focuses its beam to specific location of interest as shown in figure x. Finally, scan-SAR mode scans the antenna pattern outwards from the radar platform during each pulse to increase the width of the imaging swath.

The scattering phenomina occurring at a any target is properly described by using the electric field integral equation (EFIE) and the magnetic field integral equation (MFIE), both derivedfrom the Maxwell's equations.

The EFIE or MFIE is extremely hard to invert therefore, we have employed a scattering model that lies in between the rigorous EFIE/MFIE interpretation and the point-scattering assumption known as dipole model (DM) which not only assumes the target is collection of small dipole but also the Born approximation holds as shown in equation (4) below.

$$\begin{aligned}\mathbf{e}^{tot}(\mathbf{r}) &= \mathbf{e}^{i}(\mathbf{r}) + k_0^2 \int_V \mathbf{G}_0(\mathbf{r},\mathbf{r}') \cdot \mathbf{e}^{tot}(\mathbf{r}) \rho(\mathbf{r}') d\mathbf{r}' \\ &= \mathbf{e}^{i}(\mathbf{r}) + \mathbf{e}^{s}(\mathbf{r})\end{aligned} \quad (4)$$

where $\mathbf{e}^{s}(\mathbf{r})$ is the scattered field resulting from the interaction of the incident wave $\mathbf{e}^{i}(\mathbf{r})$ with the reflectivity function $\rho(\mathbf{r}')$, $g_0(\mathbf{r},\mathbf{r}')$ is the free space Green's function.

II. Analysis of Thin PEC Cylinder Scattering

Consider an infinite length PEC cylinder lying along the z-axis. The electrical properties are taken as homogenous and isotropic with electric and magnetic properties σ, ε, μ and have small radius a compared with the free space wavelength. The surrounding media is free space where ($\sigma = 0$, ε_0, μ_0) as shown in Figure 2. The cylinder is illuminated by a uniform incident plane wave $\mathbf{e}^{i}$, which the incident electric field is parallel to the axis of the cylinder and makes the problem entirely two dimensional.

$$\begin{aligned}&e^{i}{}_z = e_0 \exp(-jkx) \\ &where: \quad k = (\varepsilon_0 \mu_0)^{1/2} \omega\end{aligned} \quad (5)$$

k is the background wave number which specifies the direction of an incident plane wave that illuminates the target.

It is clear that when the incident wave impinging upon on the thin cylinder a current will be induced and if its sufficiently thin enough, we conclude that only the axially induced current needs to be considered. The scattered field $\mathbf{e}^{s}$ will be azimuthally symmetric and will have the form of the radiated electric field from an infinite line source

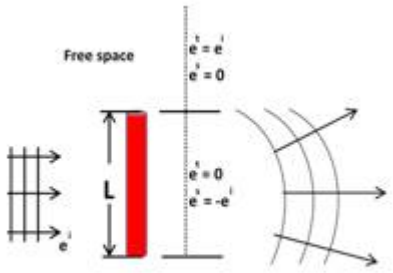

Figure 2: The behavior of electrically large object

From Maxwell's equations, one finds the electromagnetic field equations

$$\begin{aligned}&\nabla \times \nabla \times \boldsymbol{e} - k^2 \boldsymbol{e} = \boldsymbol{0} \\ &\nabla \times \nabla \times \boldsymbol{h} - k^2 \boldsymbol{h} = \boldsymbol{0}\end{aligned} \quad (6)$$

The fields consist of incident $(\boldsymbol{e}^{i}, \boldsymbol{h}^{i})$ and scattered field as well $(\boldsymbol{e}^{s}, \boldsymbol{h}^{s})$
The total fields in the surrounding media are equal to the sum of the incident and the scattered fields, i.e.

$$\begin{aligned}\boldsymbol{e}^{tot} &= \boldsymbol{e}^{i}(\boldsymbol{r}) + jk_0 \hat{\boldsymbol{r}} \times [\hat{\boldsymbol{r}} \times A] \\ &= \boldsymbol{e}^{i}(\boldsymbol{r}) + k_0^2 \int_V g_0(r,r') \cdot \mathbf{j}_{eq}(\mathbf{r}) d\mathbf{r}' \\ \boldsymbol{h}^{tot} &= \boldsymbol{h}^{i}(\boldsymbol{r}) + \boldsymbol{h}^{s}(\boldsymbol{r})\end{aligned} \quad (7)$$

where $\mathbf{j}_{eq}(\mathbf{r})$ is the induced surface current and $g_0(r,r')$ is the scalar free space far field Green's function for outgoing waves:

$$g_0(r,r') = \frac{e^{jkr}}{4\pi r} e^{-jk\hat{r}\cdot r'} \quad (8)$$

And assuming that the $\mathbf{j}_{eq}(\mathbf{r})$ is arbitrary, one can show that the homogeneous medium dyadic Green's function is the solution to the following equation

$$\nabla \times \nabla \times \bar{\mathbf{G}}(\mathbf{r},\mathbf{r}') - k^2 \bar{\mathbf{G}}(\mathbf{r},\mathbf{r}') = \bar{\mathbf{I}} \delta(\mathbf{r},\mathbf{r}') \quad (9)$$

Its solution is given below as:

$$\bar{\mathbf{G}}(\mathbf{r}/\mathbf{r}') = \left[\bar{\mathbf{I}} + \frac{\nabla\nabla}{k^2}\right] g_0(r,r') = \left[\bar{\mathbf{I}} - \hat{r}\hat{r}\right] \frac{e^{jkr}}{4\pi r} e^{-jk\hat{r}\cdot r'} \quad (10)$$

Because this dyadic Green's function generates electric field from electric current, it is also known as the electric dyadic Green's function.An electric field integral equation (EFIE) is obtained by enforcing the boundary condition for the electric field at perfectly conducting surface. The total electric field satisfies boundary condition on PEC thin cylinder:

$$n \times \boldsymbol{e}_{\tan}^{tot}\Big|_{x=R} = 0 \quad (11)$$

Upon noting that the total electric field on the surface of the PEC is the sum of the incident and scattered fields,

$$\boldsymbol{e}^{tot} = \boldsymbol{e}^{i} + \boldsymbol{e}^{s}$$

Then (12)

$$n \times \left[\int_V jk\eta_0 \mathbf{j}_{eq}(\boldsymbol{r}') \cdot \bar{\mathbf{G}}(\mathbf{r}/\mathbf{r}') \cdot d\mathbf{r}' + \boldsymbol{e}^{i}(\mathbf{r})\right] = 0$$

For $\mathbf{r} \in V$ the above equation is written as

$$-n \times \boldsymbol{e}^{i}(\mathbf{r}) = jk\eta_0 n \times \int_D \mathbf{j}_{eq}(\boldsymbol{r}') \cdot \bar{\mathbf{G}}(\mathbf{r}^t, \mathbf{r}) \cdot d\mathbf{r}' \quad (13)$$

Also the scattered field $\boldsymbol{e}^s$ and the incident field $\boldsymbol{e}^i$ both satisfy the boundary condition

$$\boldsymbol{e}^{s}\Big|_{x=R} = -\boldsymbol{e}^{i}\Big|_{x=R}$$

where: (14)

$$\boldsymbol{e}^{i}(\boldsymbol{r}) = -jk\eta_0 \int_D \mathbf{j}_{eq}(\boldsymbol{r}') \cdot \bar{\mathbf{G}}(\mathbf{r}^t, \mathbf{r}) \cdot d\mathbf{r}'$$

The incident field is the field that would exist in the computational domain in which no target exists.

III. Signal Modeling

Consider a transmitter located at $\mathbf{r}^t$ as shown in Figure 3 emitting a waveform polarized along the vector $\mathbf{a}^t$, a receiver located at $\mathbf{r}^r$ polarized along the vector $\mathbf{a}^r$, and a point under illumination at location $\mathbf{r}$. The time-harmonic incident electric field at $\mathbf{r}$ is [5]:

$$\boldsymbol{e}^{i}(\mathbf{r}, \mathbf{r}^t, \mathbf{a}^t) = \bar{\mathbf{G}}(\mathbf{r}, \mathbf{r}^t) \cdot \mathbf{a}^t$$

where: (15)

$$\bar{\mathbf{G}}(\mathbf{r}, \mathbf{r}^t) = \begin{bmatrix} G_{xx} & G_{xy} & G_{xz} \\ G_{yx} & G_{yy} & G_{yz} \\ G_{zx} & G_{zy} & G_{zz} \end{bmatrix}$$

$\bar{\mathbf{G}}$ is the free space far fields dydic Green's function of the background medium which relates the vector electromagnetic fields to vector current source and $g_0(r,r')$ is the green's function which is the solution of the field equation for a point source. Using the principle of linear superposition, the solution of the field due to general source is just the convolution of the green's function with source [4] [7].

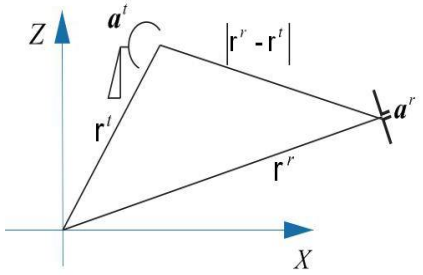

Figure 3: Source and small dipole model

Let us assume that an infinitesimally small dipole oriented along **t** is present at point **r**. When the electric field **e** impinging on **r** is parallel to **t,** then a current **j** is induced on the dipole. This current will generate a scattered field propagating in all directions, and towards the receiver antenna. The measured electric field will be [9]..

$$\boldsymbol{e}^{s} = \left(\mathbf{a}^r\right)^T \cdot \bar{\mathbf{G}}(\mathbf{r}^r, \mathbf{r}) \cdot \mathbf{j}_{eq}(\mathbf{r}) \quad (16)$$

By the way we assume that the axial current along the infinitesimal dipole is uniform. With a << λ, we may assume that any circumferential currents are negligible. The infinitesimal dipole with a constant current along its length is nonphysical antenna. However, it approximates several physical realizable antennas

Clearly, if the small dipole is not oriented along the incident field, only a fraction of the current is excited. Mathematically, the current induced in the dipole **t** can be expressed as:

$$\mathbf{j}_{eq}(\mathbf{r}) = 2\hat{n}(r') \times h^i \qquad \in s \qquad (17)$$

where $\hat{n}(r')$ is the outward unit vector of the illuminated targets surface. The vector r' is defined from the origin to any point on the illuminated surface **S**. The scattered field at the far field region along the observation vector **r** is given by

$$\boldsymbol{e}^s(\boldsymbol{r}) = -j\omega\mu \iint_S \mathbf{j}_{eq}(\boldsymbol{r}') \cdot \frac{e^{-jkr}}{4\pi r} e^{jk^s \cdot r'} \cdot d\mathbf{r}^2 \qquad (18)$$

where $\boldsymbol{k}^s = k\hat{r}$ is the wave number vector in the scattering direction. Putting equation 18 into equation 19 will yield the scattered field in terms of the incident electric field as

$$\boldsymbol{e}^s(\boldsymbol{r}) = -\frac{jk_0}{4\pi r} e^{-jk_0 r} \iint_S 2\hat{n}(\mathbf{r}') \times (\hat{k}^i \times \hat{u}) e^{j(k^s - k^i)\cdot r'} \cdot d^2\mathbf{r}'$$

(19)

This is the scattered electric field in the far field using physical optics approximation. Here k^i and k^s are the incident and scattered wavenumber vectors $\hat{n}$ is the outward surface unitary normal vector, $\hat{k}^i$ is the unit vector in the incident wave direction $\hat{u}$ is the polarization vector of the incident wave. Now let us assume that the receiving antenna has particular polarization such that it collects the scattered field in the $\hat{x}$ direction. Then we can rewrite equation 5

$$\hat{x} \cdot \boldsymbol{e}^s(\boldsymbol{r}) = -\frac{jk_0}{4\pi r} e^{-jk_0 r} \iint_S \boldsymbol{v}(\mathbf{r}') e^{j(k^s - k^i)\cdot r'} \cdot d^2\mathbf{r}' \qquad (20)$$

where $\boldsymbol{v}(\mathbf{r}')$ is the contrast function which is expressed as

$$\boldsymbol{v}(\mathbf{r}') = \hat{x} \cdot \left[2\hat{n}(\boldsymbol{r}') \times (\hat{k}^i \times \hat{u}) \right] \cdot \delta(S(r')) \qquad (21)$$

By using the dyadic notation, we can write the above equation as a discrete form as

$$\boldsymbol{e}^s = \sum_{n=1}^{P} \left(\mathbf{a}^r\right)^T \cdot \bar{\mathbf{G}}\left(\mathbf{r}^r, \mathbf{r}_n\right) \cdot \boldsymbol{v}_{k,\hat{r}}(\mathbf{r}_n) \cdot \bar{\mathbf{G}}\left(\mathbf{r}_n, \mathbf{r}^t\right) \cdot \mathbf{a}^t \qquad (22)$$

where*D* is the domain of interest $\mathbf{r}_n$ is the location of the *n*th pixel , *P* is the total number of pixels, and $\boldsymbol{v}_{k,\hat{r}}(\mathbf{r}_n)$ is the unknown contrast function which looks like as follows:

$$\boldsymbol{v}_{k,\hat{r}}(\mathbf{r}_n) = \begin{bmatrix} v_{xx} & v_{xy} & v_{xz} \\ v_{yx} & v_{yy} & v_{yz} \\ v_{zx} & v_{zy} & v_{zz} \end{bmatrix} \qquad (23)$$

IV. Inversion Technique

Mathematically, the problem of finding the reflectivity function profile is to compute the inverse linear operator of equation (22). The DM is based on the forward scattering model which relates the unknown reflectivity function $\boldsymbol{v}$ to the simulated signal. However, equation (22) returns the value corresponding to a single measurement. Therefore, by expanding let us collect a set of measurements which takes into account for all frequencies and locations for both transmitter (Tx) and receivers (Rx). For a specific measurement *m* and a specific pixel *p*, equation (22) can be modified as follows:

$$\begin{aligned} e_{mp} &= l_{mp}^{xx} v_{mp}^{xx} + l_{mp}^{xy} v_{mp}^{xy} + l_{mp}^{xz} v_{mp}^{xz} + \ldots \\ &\quad + l_{mp}^{yx} v_{mp}^{yx} + l_{mp}^{yy} v_{mp}^{yy} + l_{mp}^{yz} v_{mp}^{yz} + \ldots \\ &\quad + l_{mp}^{zx} v_{mp}^{zx} + l_{mp}^{zy} v_{mp}^{zy} + l_{mp}^{zz} v_{mp}^{zz} \\ &= \mathbf{l}_{mp}^T \cdot \boldsymbol{v}_{mp} \end{aligned} \qquad (24)$$

where, $\mathbf{e}^s$ is a (known) vector containing all measurements collected at different positions / directions / frequencies, **L** is a (large) matrix whose entries can be calculated theoretically from (22), and $\boldsymbol{v}$ is a vector representing the dyadic reflectivity function of the target. By employing back-projection technique, the reflectivity function can be easily retrieved [10]:

$$\boldsymbol{v} \cong \mathbf{L}^H \mathbf{e}^s \qquad (25)$$

V. Simulation Results

In this paper, we performed 2D and 3D simulation with multiple orientations. In case1, a thin cylinder (representing a wire) is oriented horizontally along x-axis and case2, it is oriented along the y-axis and in case3, it is oriented vertically at the center along z-axis. All three cases the transmitting and receiving antennas are located in the x-y plane. In the

simulation we used 30 transmitters and 100 receivers both which the transmitters and receivers transmit and receive in all three orthogonal polarizations such as $(\hat{\mathbf{x}}, \hat{\mathbf{y}}\ and\ \hat{\mathbf{z}})$. The transmitting antennas are placed along a radius of 13λ and the receiving antennas are also placed 10λ with respect to the target. The operating frequency is 10 GHz $(\lambda = 3cm)$ and the total measurement collected from this is $(N_t \times N_r = 30*100 = 3000)$; where N_t and N_r are number of transmitters and number of receivers. The area of investigation is 0.4 m by 0.4 m which divided into pixels with size of 0.05λ .

The goal of this simulation is to obtain a) the oriantation of the target based on co-polarization and b) is to reconstruct the 2D & 3D of the target of interest as shown figures below.

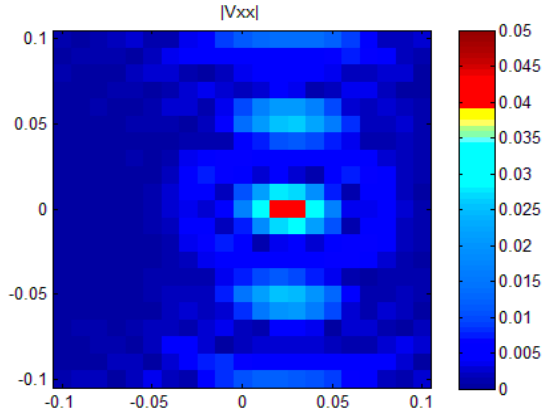

Figure 4: The image of the cylinder is located along x-axis (0 $\leq$ x $\leq$ 5).

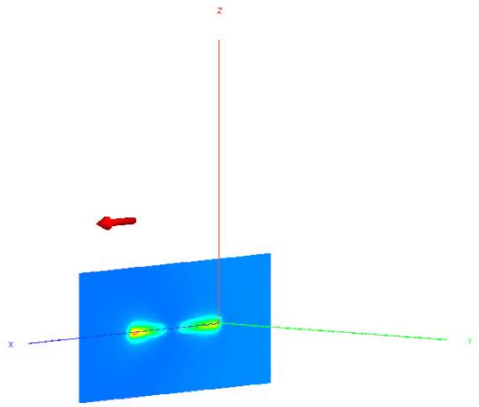

Figure 5: Near field Radiation along x-axis

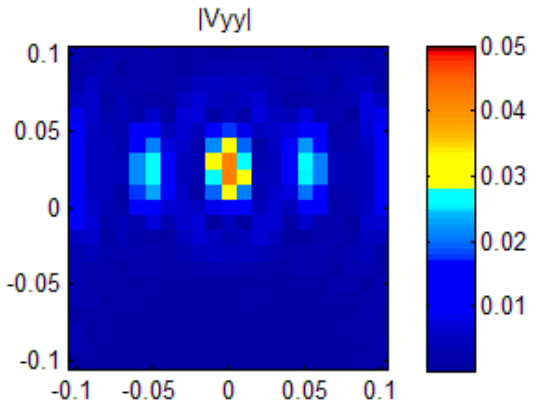

Figure 6: The image of the cylinder is located along y-axis (0 $\leq$ y $\leq$ 5).

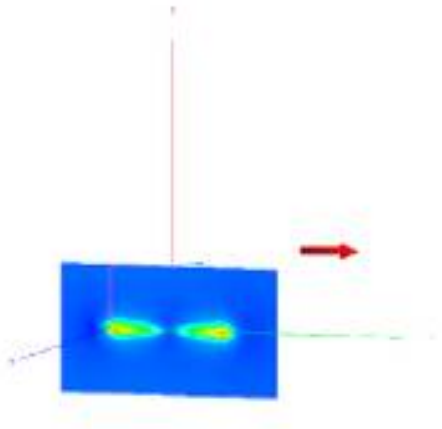

Figure 7: Near field Radiation along y-axis

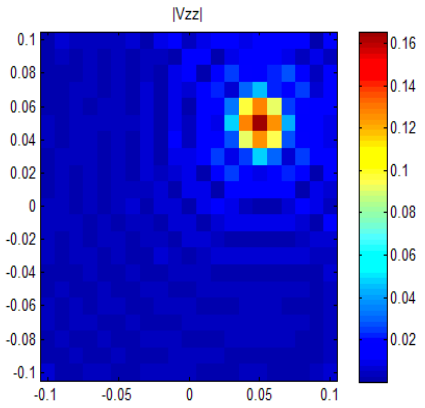

Figure 8: The image of cylinder located at (x = y = 5 cm) along z- direction

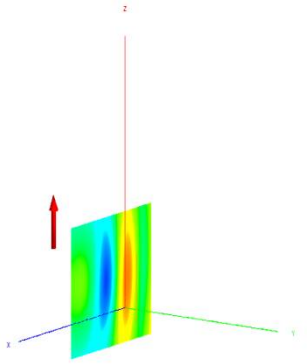

Figure 9: Near field Radiation along z-axis

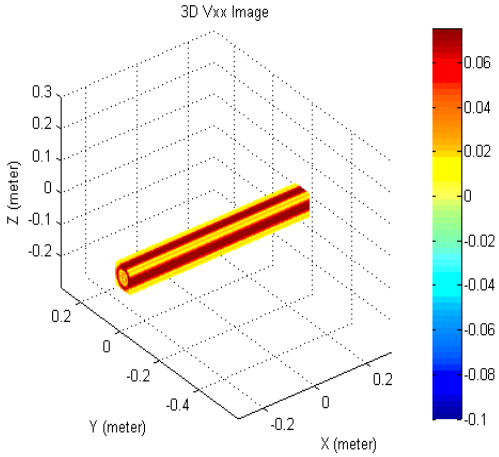

Figure 10: 3D image of horizontally oriented cylinder. The cylinder and the antenna are both oriented along x - axis. The target is detected due to the same alignment with incident field.

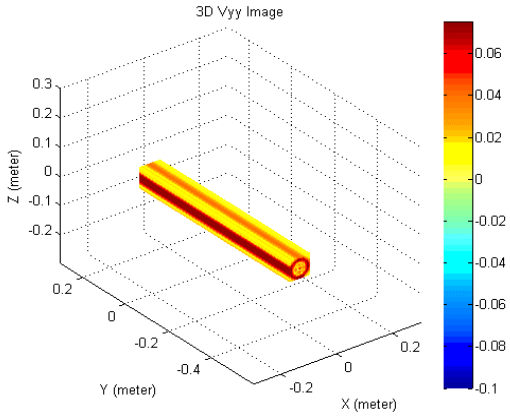

Figure 11: 3D image of horizontally oriented cylinder. The cylinder and the antenna are both oriented along y - axis. The target is detected due to the same alignment with incident field.

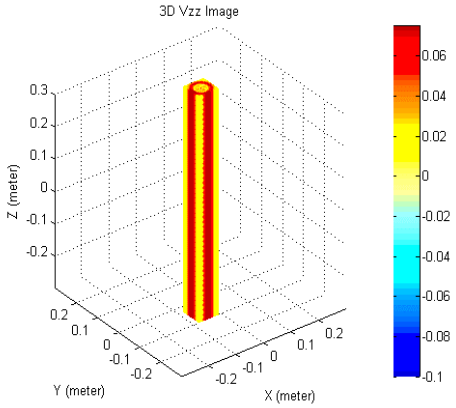

Figure 12: 3D image of vertically oriented cylinder. The cylinder and the antenna are both oriented along z - axis. The target is detected due to the same alignment with incident field

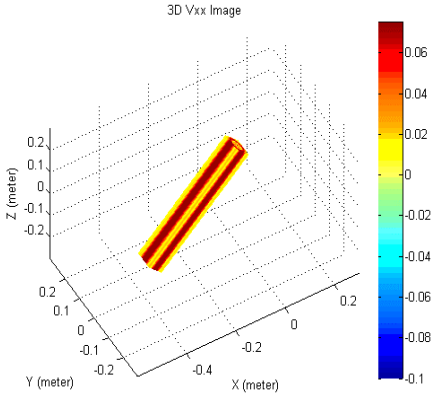

Figure 13: Both the antenna and the cylinder are rotated by +45 along x-axis and detection occurs.

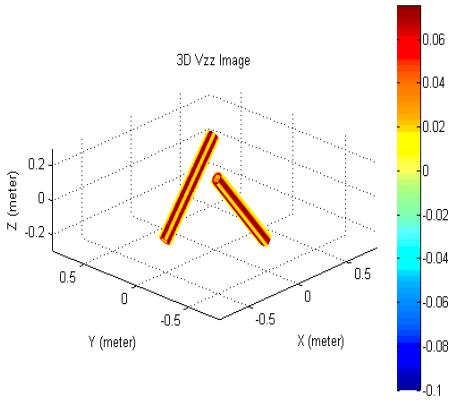

Figure 14: Two cylinders, first one is rotated -45 and the second on is rotated +45

Conclusions

In this paper we seccessfully imaged a thin cylinder with multiple oriantations in 2D & 3D. Under the dipole model based approach, detection declaration occurred only when the antenna and the cylinders are co-polar, as shown in all the figures.

References

[1] R. L. Moses, L. Potter and M. Cetin, "Wide Angle SAR Imaging," in *SPIE Defense and Security Symposium*, 2004.

[2] C. A. Balanis, Advanced Engineering Electromagnetics, John Wiley & Sons, 1989.

[3] M. Gustafsson, "Multi-Static Synthetic Aperture Radar and Inverse Scattering," LUTEDX/(TEAT-7123)/1-28/(2003), 2004.

[4] J. A. Jackson, Three-Dimensional Feature Models for Synthetic Aperture Radar and Experiments in Feature Extraction, Columbus, OH: PhD Dissertation, The Ohio State University, 2009.

[5] M. Almutiry, A. Nassib, Y. Guzel, T. Negishi, D. Erricolo, M. C. Wicks and L. L. Monte, "Exploitation of Dominant Scatterers for Sidelobe Suppression in Radar Tomography," in *Signal Processing Symposium 2015 June 10 - 12 2015*, Debe, Poland.

[6] L. Lo Monte, F. Soldovieri, D. Erricolo, A. Giannopoulos and M. C. Wicks, "A Comprehensive Forward Model for Imaging under Irregular Terrain Using RF Tomography," *nternational Journal of Antennas and Propagation*, vol. Volume 2012, p. 15, 2012.

[7] L. Lo Monte, F. Soldovieri and M. C. Wicks, "Radio Frequency Tomography for Tunnel Detection," *IEEE TRANSACTIONS ON GEOSCIENCE AND REMOTE SENSING*, vol. VOL. 48, p. NO. 3, MARCH 2010.

[8] M. S. Zhdanov, Geophysical Inverse Theory and Regularization Problems,Methods in Geochemistry and Geophysics, Elsevier Science, May 8, 2002.

[9] B. BORDEN, Fundamentals of Radar Imaging, Philadelphia,: SOCIETY FOR INDUSTRIAL AND APPLIED MATHEMATICS, 10/8/2009.

[10] R. T. f. G. P. R. S. a. Experimentation, "Yasar Guzel;Thang Tran;Ali Nassib;Muhannad Almutiry;M. C. Wickw;L.Lo Monte," in *IEEE Rradar Conference 2015*, Arlington VA.

[11] a. Nassib, M. Almutiry, Y. Guzel, M. Michael and L. Lo Monte, "FEKO Based ISAR Analysis for 3D Object Reconstruction," in *IEEE radar conference* , Arlington, 2015.

[12] V. Picco, T. Negishi, S. Nishilata, D. Spitzer and D. Erricolo, "RF Tomography in Free Space: Experimental Validation of the Forward Model and an Inversion Algorithm Based on the Algebraic Reconstruction Technique," *International Journal of Antennas and Propagation*, Vols. Volume 2013 ,Article ID 528347, p. 9, 2013.

[13] M. C. Wicks, "RF Tomography with Application to Ground Penetrating Radar," in *Signals, Systems and Computers, 2007. ACSSC 2007*, Pacific Grove, Ca, Nov. 2007.

[14] L. Lo Monte, F. Soldovieri and M. C. Wicks, "Radio Frequency Tomography for Tunnel Detection," *IEEE Transactions on Geosciences and Remote Sensing*, vol. VOL. 48, p. NO. 3, MARCH 2010.

[15] B. J. WEI and Q. H. LIU, "Fast Algorithm for Simulating 3-D Electromagnetic Inverse Scattering in Horizontally Stratified medium via DTA," *CHINESE JOURNAL OF GEOPHYSICS*, vol. Vol.50, p. No.5, 2007.

[16] J. C. Tie and C. C. Weng, "Diffraction Tomographic Algorithm for the Detection of Three-Dimensional Objects Buried in a Lossy Half-Space," *IEEE TRANSACTIONS ON ANTENNAS AND PROPAGATION*, vol. VOL. 50, JANUARY 2002.

[17] W. Rieger, M. Haas, C. Huber, G. Lehner and W. Rucker, "Inverse electromagnetic medium scattering using a variable metric method," in *Antennas and Propagation Society International Symposium*, Montreal, Quebec Canada, July 1997.

[18] A. Nassib, T. Negishi, D. Erricolo, M. Wicks and L. Lo Monte, "A Dyadic Target Model for Multistatic

SAR/ISAR Imaging," in *2015 IEEE International Radar Conference*, Arlington, 2015.

[19] S. Z. Michael, Geophysical Inverse Theory and Regularization Problems,Methods in Geochemistry and Geophysics, Elsevier Science, May 8, 2002.

[20] L. Lo Monte, F. Soldovieri and M. C. Wicks, "RF Tomography for Below-Ground Imaging of Extended Areas and Close-in Sensing," *IEEE GEOSCIENCE AND REMOTE SENSING LETTERS*, vol. VOL. 7, p. NO. 3, JULY 2010.

[21] I. LaHaie and B. Fischer, "T13 — Transformations for Radar Cross-Section (RCS) and imaging from monostatic near-field measurements," in *Radar Conference, 2014 IEEE*, Cincinnati, Ohio, May 2014.

[22] J. A. K. a. K. H. D. L. Tsang, Scattering of ElectromagneticWaves,Theories and Applications, New York: Wiley-Interscience, 2004.

[23] P. C. C. C. E. K. B. a. P. S. J.-M. Geffrin, "Electromagnetic three-dimensional reconstruction of targets from free space experimental data," *Applied Physics Letters*, vol. vol. 92, no. Article ID 194103, p. no. 19, 2008.

[24] W. C. Chew, Waves and Fields in Inhomogeneous Media, New York: IEEE Press, 1995.

[25] C. A. Balanis, Advanced Engineering Electromagnetics, John Wiley & Sons, 1989.

[26] J. T. Parker, M. Ferrara, J. Bracken and . B. Himed, "Preliminary experimental results for RF tomography using distributed sensing," in *Proceedings of the 12th International Conference on Electromagnetics in Advanced Applications (ICEAA '10), pp.549–552*, September 2010.

[27] C. OZDEMIR, INVERSE SYNTHETIC APERTURE RADAR IMAGING WITH MATLAB ALGORITHMS, Hoboken,New Jersey: John Wiley & Sons, 2012.

[28] T. H. Chu and D. B. Lin., "Microwave diversity imaging of perfectly conducting," *IEEE Trans Microwave Theory Tech*, no. 39, p. 480–487, 1991.